

# **Location-dependency of green density and dimension variation in binder jetted parts**

Maciej Dorula <sup>a,1</sup>, Meisam Khademitab <sup>a</sup>, Mohammad Jamalkhani <sup>a</sup>, Amir Mostafaei <sup>a,\*</sup>

<sup>a</sup> Department of Mechanical, Materials and Aerospace Engineering, Illinois Institute of Technology, 10 W 32<sup>nd</sup> Street, Chicago, IL 60616, USA

<sup>1</sup> REU summer student awarded by National Science Foundation

\*Corresponding author: A. Mostafaei

Email: [mostafaei@iit.edu](mailto:mostafaei@iit.edu)

## **Abstract**

Binder jetting is a powder bed additive manufacturing process where an object is created by depositing liquid binder onto the surface of powder, selectively binding particles in each layer. The quality of the as-printed parts is influenced not only by process parameters such as layer thickness, binder saturation, print speed, and drying time but also by the location within the build box. This study highlights the location-dependent nature of green density and dimensional accuracy in the as-printed samples, and the observed trends are thoroughly discussed. A conventional powder spreading using a single roller was compared with a double roller to maximize powder packing and bed uniformity prior to binder jetting process. The significance of these observations lies in their impact on densification behavior, shrinkage, and the final geometry of the printed part.

## **Keywords**

Additive manufacturing; Powder dispenser; Powder compaction; Green density; Dimensional tolerance.

## **1. Introduction**

Binder jetting is a powder bed additive manufacturing (AM) process that involves binding powder together using a polymeric binder based on a computer-aided design (CAD) model. The resulting 3D printed part, known as the green part, undergoes curing in an oven to improve its

strength. Binder jetting offers advantages over other AM methods, including geometric flexibility, minimal support structure requirements, diverse material options, high scalability, and low machine costs [1]. The green parts initially contain ~40-60% porosity, necessitating post-processing known as consolidation to achieve the desired relative density. For structural materials, sintering is a common method used to eliminate pores, involving shrinkage and deformation in the final parts. Prior to sintering, debinding at 450-600 °C for 30-60 min is a crucial step to burnout the binder and minimize carbon contamination in the final densified parts. In the final stage of sintering, two typical sintering mechanisms are employed: (1) solid-state sintering, where the applied temperature is kept below the solidus temperature [2,3], and (2) supersolidus liquid phase sintering, where the applied temperature is slightly above the solidus temperature to form a small fraction of liquid metal, aiding densification [4,5]. The latter is an effective consolidation process that enhances relative density above 99%.

While the binder constitutes only about 1% of the total weight of 3D printed parts, its influence on the properties of the green parts is substantial. The chemical stability, rheology, wettability with the powder bed, and binding strength of the polymer binders used in binder jet machines are crucial factors [6]. Additionally, process variables such as binder saturation, droplet spacing, and binder velocity need optimization based on powder morphology and size metrics [7]. The three primary characteristics—powder morphology, mean size, and distribution—directly impact powder spreading, the dynamics of powder-binder interaction, and the final consolidated part [6,8–10]. Other process parameters, including layer thickness and print speed, affect powder packing and green densities [11]. Typically, the layer thickness can range from 20  $\mu\text{m}$  to 200  $\mu\text{m}$ , with a suggestion to set it 2-3 times the powder mean size [1,12]. The effects of faster print speeds on part outcomes are not yet fully understood. Myers et al. [13] observed that as the spread speed increased from 3 mm/s to 125 mm/s, the green density decreased from 52.7% to 50%. Oropeza et al. [14], employing transmission x-ray imaging for spatially-resolved, non-contact powder layer density measurements, studied the effects of various variables on powder spreading, revealing complex relationships between powder characteristics and process parameters. They studied the impact of multiple variables on powder spreading, including factors such as powder size and shape, the choice of spreading tools (e.g., blade versus roller), traverse speed and/or rotation rate, and powder dispensing methodology (i.e., piston-fed vs hopper). The outcomes revealed intricate relationships between powder characteristics and process parameters.

Critical benchmarks for binder jetted parts include achieving uniformity in green density and dimensional tolerance, both of which are directly influenced by powder characteristics and process parameters. The consolidation process, particularly through sintering, is significantly impacted by these criteria, as inconsistency in green density and the presence of internal defects may lead to deformation [15–20]. Over the past two decades, binder jet systems have undergone various advancements, ranging from improvements in powder dispensing methods and compaction to enhanced printhead resolution and dimensional accuracy. While many studies have focused on printing single layer coupons with heights up to 2 cm in the build box, providing average green density figures, a notable gap exists as the green density and dimensional tolerance have not been reported as functions of location. This research not only highlights potential challenges in binder jetting systems but also proposes viable solutions to mitigate such deviations.

## 2. Materials and Experiments

In this study, spherical gas atomized powders, as an exemplary system Co-Cr-Mo, were supplied by Kennametal Inc. with the particle size distribution between 15–45  $\mu\text{m}$  with a mean size of 32.0  $\mu\text{m}$ . Binder jet 3D printing process of the specimens have been implemented by ExOne printers, including Innovent and Innovent<sup>+</sup> using optimum process parameters given in Table 1. To understand location dependency of green parts of binder jetted specimens, coupons with dimensions of  $10 \times 10 \times 10 \text{ mm}^3$  were laid out in the job box as illustrated in Figure 1. A total of 4 layers including 40 coupons in each layer was designed in the job box. A polymeric binder (BA-005 water-based binder, ExOne, which works well with a variety of metallic materials) uniformly jetted onto the powder bed. The used printhead in the Innovent and Innovent<sup>+</sup> printers were named as 80-pL and 30-pL, respectively. After completion of binder jetting process, the job box was placed in a curing oven and the temperature was set at 185 °C for 8 h. Then, coupons were depowdered and detailed analysis including mass (using OHAUS Scout® balance scale with 0.1 mg accuracy) and dimensional measurements (using a digital caliper with 10  $\mu\text{m}$  resolution) were carried out on every single specimen. The role of powder dispensing method on the packing density of the used powder was assessed by print cup tests [21] with inner vacant volumes of  $15 \times 15 \times 15 \text{ mm}^3$ .

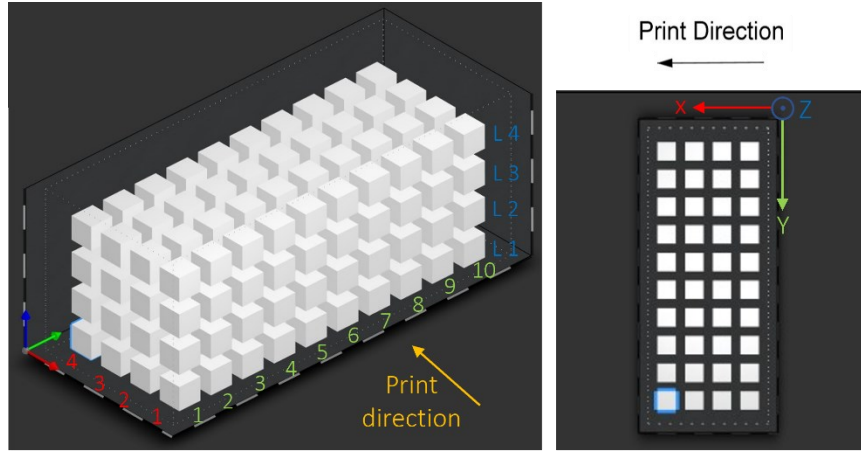


Figure 1. Schematics illustrating the build layouts and position of coupons throughout the entire print.

Table 1. Specified optimum process parameter inputs for the used powder in ExOne Innovent and Innovent<sup>+</sup> binder jetting printers.

Parameter/input	Optimum set values	
	Innovent	Innovent <sup>+</sup>
Layer thickness (µm)	75	75 µm
Binder saturation (%)	70	70
Drying time (s)	15	10
Recoat speed (mm/s)	120	40
Bed temperature (°C)	40	40
Emitter output (%)	60	100
Oscillation speed (rpm)	2500	-
Roller rotation speed (rpm)	350	-
Roller traverse speed (mm/s)	15	-
Smoothing roller speed (rpm)	-	400
Roughing roller speed (rpm)	-	200
Roller traverse speed (mm/s)	-	3
Intensity of ultrasound vibrator (%)	-	15
Binder set time (s)	-	8

### 3. Results and discussion

In binder jetting, the gravitational force of each layer and the repetition of the rolling process increase the green density of the bottom layers. Therefore, deeper layers potentially have higher green density compared to the upper layers; in other words, traveling in the Z direction reduces the green density of the coupons. In addition, it was reported that the green density of the binder jetted parts within the same Z height showed deviation in relative densities [1], thus, reducing repeatability of manufacturing final sintered parts with predictable shrinkage, final density and properties. Here, we initially present results of the produced green parts pertaining to the ExOne Innovent printer, followed by insights from the Innovent<sup>+</sup> printer. This discussion delves into the

process-dependent nature of location dependency concerning green density and dimensional accuracy during binder jetting.

**Innovent printer** - Figure 2(A) demonstrated the abovementioned phenomenon in which the very bottom layer ( $L_1$ ) of the binder jetted coupons had higher green density (up to 2.5%) compared to the top layer specimens. A green density reduction was observed by moving from the first layer on the bottom to the final layer on the top in the order of  $L_1 > L_2 > L_3 > L_4$  ( $52.2 \pm 0.4\% > 51.4 \pm 0.5\% > 50.8 \pm 0.4\% > 50.6 \pm 0.5\%$ ). Also, the green density values were higher in specimens located near the walls (front, back and right side of the job box) compared to the center and left wall.

The dependency of weight as a function of location in binder jetted parts was shown in Figure 2(B). A similar behavior to the green density measurement was observed in mass measurements in which binder jetted parts close to the right, front and back walls showed higher weight compared to the center and left wall locations. This inconsistency can be explained by two factors. First, the walls play as a barrier towards loose powder and prevent them from scattering when the roller tries to compact and smooth each powder spread layer. Hence, the packing density near the walls could be increased. We found that the packed loose powder has a relative density of  $\sim 60.3 \pm 0.9\%$  close to the wall on the right side of the built while it decreased to  $58.5 \pm 1.2\%$  close to the left wall. Second, the amount of fine powder at the beginning of the rolling process (right wall) is more than those in other locations. Therefore, the fine powder could fill more voids than the coarse powder and the packing density could be higher near the walls. Likewise, the changes regarding the mass of the coupons can be justified. As the powder spread proceeds to the left side of the job box, the total mass of powder as well as fine powder in the spread layer decreases, thus, the packing density is lightly lower on the left side of the job box.

Regarding dimensional accuracy in different directions, it was shown in Figure 2(C) that the dimensional tolerance in the  $X$  direction (roller travel direction) is almost uniform in all layers in which the range was between 10.08 mm and 10.18 mm ( $\sim 1\text{-}2\%$  higher than the CAD model). The average and standard deviation of the measured length in  $X$  direction for  $L_1$  to  $L_4$  was  $10.117 \pm 0.018$  mm,  $10.121 \pm 0.022$  mm,  $10.120 \pm 0.031$  mm, and  $10.126 \pm 0.032$  mm. Three aspects can affect this behavior. First, the shear force caused by roller traverse movement in  $X$  direction can slightly shift powder on each layer. Second, the lateral binder permeation may cause loose powder from the bed to stick to the side surfaces of binder jetted parts, thus, adds up to the  $X$  direction. Third, the

deposited binder may displace powder in *X* direction which also leads to in-layer voids and potentially increased dimensional tolerance in the *X* direction.

On the *Y* direction, three distinct regions were visible on Figure 2(D). First, binder jetted parts close to the back wall had slightly higher tolerance in *Y* direction, between 10.15 mm and 10.05 mm, then the location-dependency became less sensitive up to close to the center of the job box in which the length in *Y* direction was ranging between 10.00 mm and 10.05 mm. Second, a slight reduction dimension was seen in coupons printed in the middle towards the front wall in which the length in *Y* direction was between 9.96 mm and 10.00 mm. Third, by getting closer to the front wall, the length tolerance in *Y* direction was between 10.00 mm and 10.05 mm. Overall, the length of the printed coupons was closer to the CAD model in *Y* direction compared to the *X* direction. This could be because binder spraying, and roller traverse movement had minimal impact on binder permeation and powder displacement in *Y* direction. The average and standard deviation of the measured length in *Y* direction for L<sub>1</sub> to L<sub>4</sub> was 10.018±0.018 mm, 10.121±0.022 mm, 10.28±0.041 mm, and 10.034±0.041 mm.

The result of measured dimensions in *Z* direction was demonstrated in Figure 2(E). Two behaviors were obvious on the contour plots. First, the gravitational force of the upper layers and higher compaction by the rollers resulted in height tolerance between 9.9 mm and 10 mm on the bottom layer (L<sub>1</sub>), while the dimensional variations increased at upper layers. For instance, it was seen that the height of samples was between 10.00 mm and 10.15 mm on the 3<sup>rd</sup> layer (L<sub>3</sub>) and it was between 10.05 mm and 10.20 mm on the top layer (L<sub>4</sub>). Second, it was observed that the height of specimens located on the right side of the job box was slightly higher than the left side in layers L<sub>1</sub> and L<sub>2</sub>. This was thought to be related to higher packing rate of powders on the right side due to the presence of both fine and coarse powder, while, by moving to the left side, packing density slightly decreases and results in less compacted powder in each spread layer. Thus, movement of roller on the next layer of powder could slightly pack previous layers and reduce height. On the very top layer (L<sub>4</sub>), the opposite behavior was seen. This could be because of the lower number of stacked powder layers when coupons in L<sub>4</sub> were binder jetted, thus, gravitational force was not significant on the left side of the job box to further pack powder. The average and standard deviation of the measured length in *Z* direction for L<sub>1</sub> to L<sub>4</sub> was 9.980±0.025 mm, 10.024±0.029 mm, 10.066±0.027 mm, and 10.106±0.034 mm.

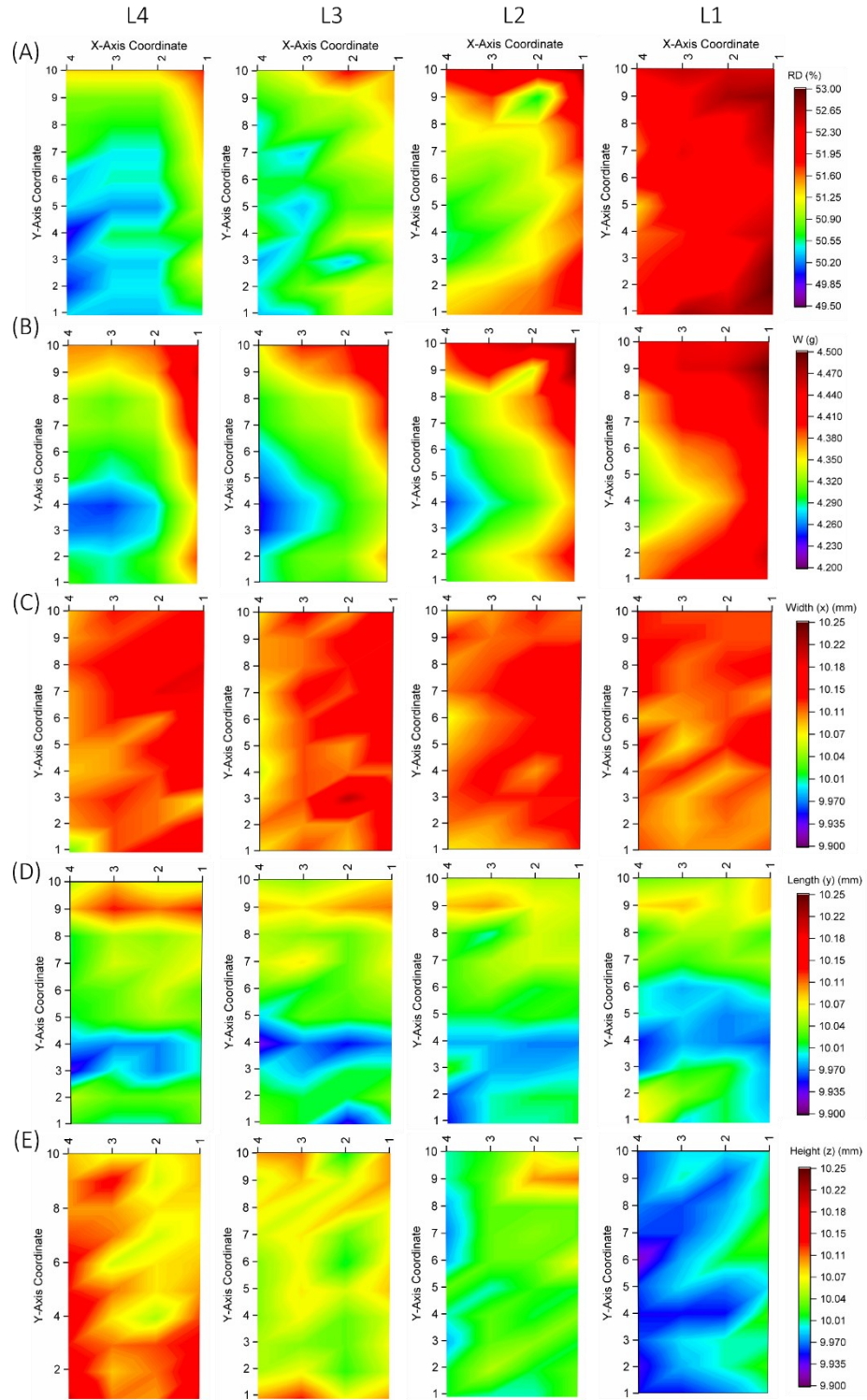


Figure 2. *Innovent printer*: (A) Green density contour plot for binder jetted metal powder at different locations on the job box. The green density measurement was based on the mass and dimension measurements. (B) Weight contour plot for binder jetted metal powder at different locations on the job box. The weight measurements were carried out using a scale with 0.01 mg accuracy. Tolerance in (C)  $X$  direction, (D)  $Y$  direction, and (E)  $Z$  direction contour plots for binder jetted metal powder at different locations on the job box. The dimension measurements were carried out using a caliper with 10  $\mu\text{m}$  resolution.

**Innovent<sup>+</sup> printer** – Given the inconsistencies in relative densities and dimensional accuracies observed in conventional powder dispensing using a single roller in binder jet printers, such as Innovent, there is a need to enhance powder compaction and bed uniformity. This improvement can be achieved by incorporating double rollers, including a roughing roller and a smoothing or finishing roller. Although this new powder dispenser has been implemented on the ExOne Innovent<sup>+</sup> printer by the ExOne Company, a crucial gap exists in the absence of a side-by-side comparison of efficiency and accuracy between printers. This concern becomes particularly critical when dealing with the binder jetting of complex, massive parts, where unexpected shrinkage in three dimensions and deformation pose significant challenges to geometry accuracy of the sintered parts. Figure 3 demonstrated our measurements of the relative densities, mass, and dimensions of binder jetted parts using the double roller powder dispenser.

In terms of the relative density of the green parts (depicted in Figure 3(A)), it was observed that the very bottom layer ( $L_1$ ) of the binder jetted coupons exhibited a higher green density (up to 1.5%) compared to the top layer specimens ( $L_4$ ). A reduction in green density was noted moving from the first layer at the bottom to the final layer at the top in the order of  $L_1 > L_2 > L_3 > L_4$  ( $57.1 \pm 0.2\% > 56.5 \pm 0.4\% > 56.0 \pm 0.3\% > 55.5 \pm 0.3\%$ ). Additionally, the measured green density values showed less dependency on location within each layer opposed to the observations and measurement of the 3D printed samples using conventional powder dispenser in the Innovent printer. The dependency of weight as a function of location in binder jetted parts was illustrated in Figure 3(B), and a similar trend as the green density was observed.

The enhancement in weight, green density, and consistency in each layer of binder jetted samples can be explained by the fact that the double rollers improved powder packing density (referring to the packed loose powder) to  $64.0 \pm 0.8\%$ , which was about 4% higher compared to the single pass roller. Moreover, the applied second pass roller, including height reduction of deposited powder layer ( $\Delta h$ , discussed later in this paper in Figure 4) and powder compaction in this step, further assisted bed uniformity and packing density of powder in each discrete deposited layer. Thus, as the powder spread proceeds in each layer with a certain layer thickness, the total mass of deposited powder becomes higher in this new dispensing approach.

Concerning dimensional accuracy in different directions, as illustrated in Figure 3(C), the dimensional tolerance in the *X* direction (roller travel direction) remained consistent across all layers, ranging between 10.08 mm and 10.10 mm (~1% higher than the CAD model). The average and standard deviation of the measured length in the *X* direction for L<sub>1</sub> to L<sub>4</sub> were 10.103±0.017 mm, 10.100±0.017 mm, 10.090±0.017 mm, and 10.090±0.017 mm. As previously discussed for the Innovent printer, the shear force induced by roller traverse movement in the *X* direction could slightly shift powder on each layer. Additionally, lateral binder permeation might cause loose powder from the bed to adhere to the side surfaces of binder jetted parts, contributing to the *X* direction. Finally, the deposited binder could displace powder in the *X* direction, leading to in-layer voids and potentially increased dimensional tolerance in the *X* direction. However, the length measurements in the *X* direction demonstrated minimal deviation in the Innovent<sup>+</sup> printer including the double roller, and coupons exhibited more or less similar lengths in the *X* direction.

In the *Y* direction, the dimensional tolerance remained uniform across all layers, as depicted in Figure 3(D). This finding contradicted our previous findings with the conventional single roller. The average and standard deviation of the measured length in the *Y* direction for L<sub>1</sub> to L<sub>4</sub> were 10.023±0.018 mm, 10.023±0.019 mm, 10.033±0.023 mm, and 10.036±0.019 mm. This suggested that the length of the printed coupons was closer to the CAD model in the *Y* direction compared to the *X* direction. This could be attributed to the fact that binder spraying, and roller traverse movement had minimal impact on binder permeation and powder displacement in the *Y* direction.

The result of measured dimensions in *Z* direction was demonstrated in Figure 3(E). Similar to the single roller printing condition, the gravitational force of the upper layers and higher compaction by the rollers resulted in height tolerance between 9.96 mm and 10.02 mm on the bottom layer (L<sub>1</sub>), while the dimensional variations increased at upper layers. For instance, it was seen that the height of samples was between 9.98 mm and 10.05 mm on the 2<sup>nd</sup> layer (L<sub>2</sub>), 10.01 mm and 10.10 mm on the third layer (L<sub>3</sub>), and 10.06 mm and 10.13 mm on the top layer (L<sub>4</sub>). The height of specimens in each discrete layer of the job box was almost the same. The average and standard deviation of the measured length in *Z* direction for L<sub>1</sub> to L<sub>4</sub> was 9.991±0.017 mm, 10.017±0.019 mm, 10.058±0.024 mm, and 10.094±0.017 mm.

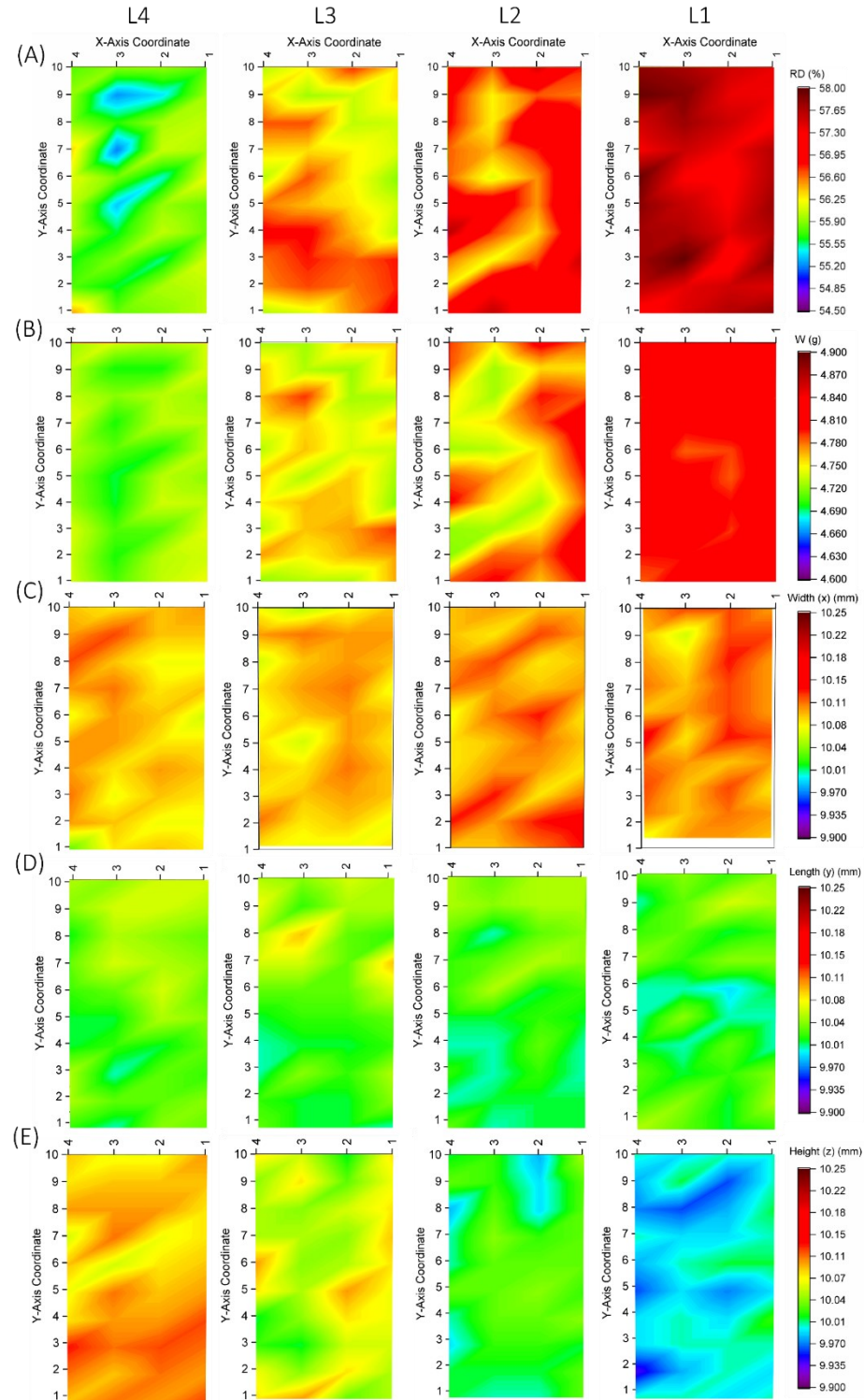


Figure 3. *Innovent<sup>+</sup>* printer: (A) Green density contour plot for binder jetted metal powder at different locations on the job box. The green density measurement was based on the mass and dimension measurements. (B) Weight contour plot for binder jetted metal powder at different locations on the job box. The weight measurements were carried out using a scale with 0.01 mg accuracy. Tolerance in (C) *X* direction, (D) *Y* direction, and (E) *Z* direction contour plots for binder jetted metal powder at different locations on the job box. The dimension measurements were carried out using a caliper with 10  $\mu$ m resolution.

To illustrate the distinction between the two powder dispensing methods employed in the Innovent and Innovent<sup>+</sup> printers, Figure 4 presents schematics of each method. The powder spreading system on the Innovent printer involves a hopper that oscillates to sieve powder onto the powder bed, followed by a roller that swipes and compacts the powder, see Figure 4(A). In this printer, powder is sieved on only 1/3 of the build on the right side, and the roller's task is to spread powder across the entire surface. It is typically assumed that the powder size distribution is more uniform or Gaussian on the right side of the build; however, powder segregation can occur as the roller spreads powder from one side to the other, resulting in a slightly lower population of fine powder on the left side. This was observed in our examination of binder jetted parts using the Innovent printer (Figure 2).

In contrast, the powder spreading system in the Innovent<sup>+</sup> printer involves an ultrasonic dispenser, and the hopper moves over the entire build, sieving powder onto the entire surface. Subsequently, the double roller powder dispensing configuration shown in Figure 4(B), comprising a roughing roller and smoothing roller, spreads and compacts the powder bed. The height difference between the roughing and smoothing rollers ( $\Delta h$ ) is typically 50-100  $\mu\text{m}$ , with the smaller number being preferred. This is because the smoothing roller's responsibility is to smoothen and further compact the powder bed. A larger height difference could cause friction between powder particles and the roller, potentially leading to the shifting of deposited layers on the underlying layers.

Various process parameters, such as recoat speed, roller rotation speed, binder saturation, drying time, etc., are critical variables influencing green density and dimensional accuracy. Conflicting results have been reported regarding the role of print speed on the packing density of different powders [11,13,14,22,23]. Hence, a comprehensive study is necessary to understand how different process parameters, combined with powders of varying characteristics (size, morphology, mean size, etc.), could affect powder bed packing density, bed uniformity, and the final green density of binder jetted samples. This includes an in-situ synchrotron studies [7,24] and computation modeling [25] of the binder jetting process.

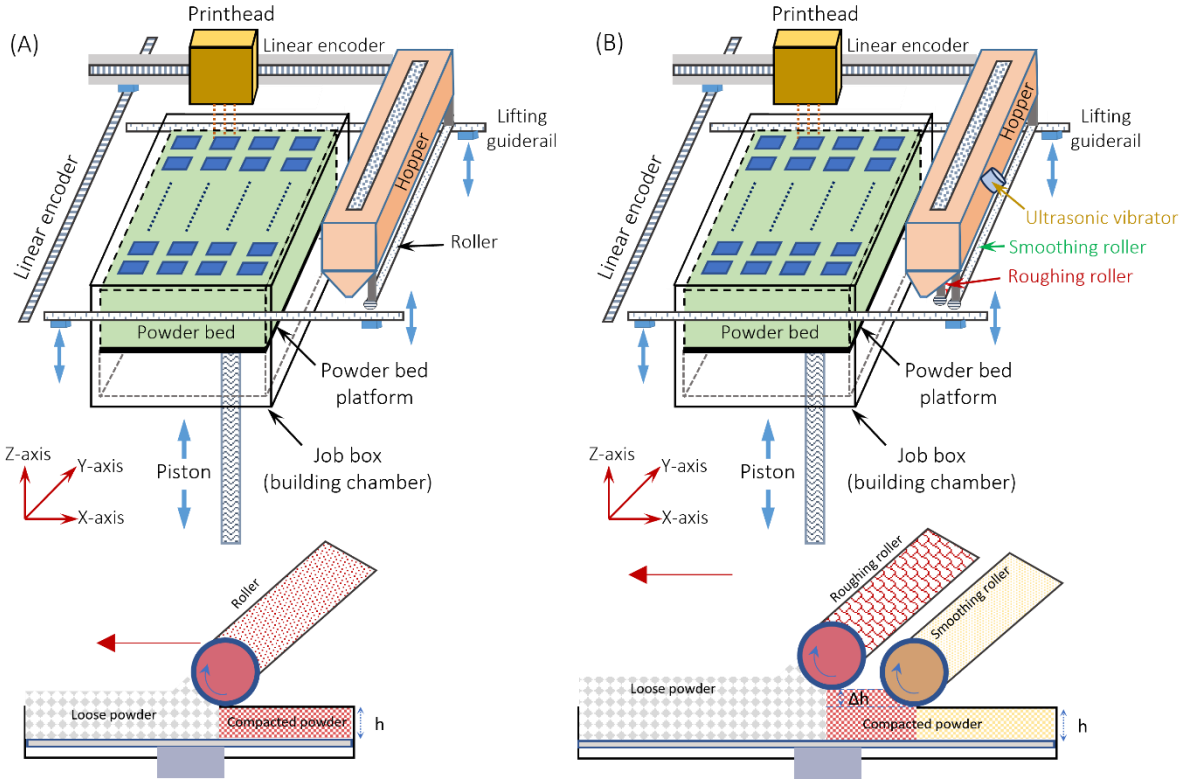


Figure 4. Schematic illustration of binder jetting in (A) Innovent and (B) Innovent<sup>+</sup> printers. A side view of powder spreading and compaction showed a comparison of how a single roller vs. double rollers -also known as Triple ACT (Advanced Compaction Technology) – affect powder bed packing density in each discrete deposited powder layer.

#### 4. Conclusions

This study aimed at understanding how powder spreading impacts location-dependency of binder jetted parts. The study conducted a comparison between the traditional method of powder spreading involving a single roller and an innovative approach using a double roller. This was intended at enhancing powder packing and ensuring uniformity in the bed before the binder jetting process. The use of a double roller in the binder jetting process resulted in a notable improvement in green density, exhibiting an increase of up to 5% compared to the conventional method with a single roller. Additionally, employing the double roller configuration enhanced dimensional accuracy across all three dimensions. The importance of these findings is highlighted by their potential effects on the densification behavior, shrinkage, and the ultimate geometry of the printed component. Essentially, the choice of powder spreading technique can play a pivotal role in shaping the final characteristics and quality of the printed parts.

## **Acknowledgments**

AM would like to acknowledge the startup funding from the Department of Mechanical, Materials and Aerospace Engineering and Armour College of Engineering at Illinois Institute of Technology at Chicago, Illinois. This research was funded, in part, by the Commonwealth of Pennsylvania's Department of Community and Economic Development (DCED), the Pennsylvania Infrastructure Technology Alliance (PITA), and the first round of the PA Manufacturing Innovation Program (PAMIP). Acknowledgments to Prof. A.D. Rollett for supporting in securing funding for this research through PITA and PAMIP. Also, Kennametal Inc. is acknowledged for providing powder for this research. Partial support from the National Science Foundation under grant number DMR-2050916 is appreciated by MD and AM.

## **Declarations**

### **Funding**

AM would like to acknowledge the startup funding from the Department of Mechanical, Materials and Aerospace Engineering and Armour College of Engineering at Illinois Institute of Technology at Chicago, Illinois. This research was funded, in part, by the Commonwealth of Pennsylvania's Department of Community and Economic Development (DCED), the Pennsylvania Infrastructure Technology Alliance (PITA), and the first round of the PA Manufacturing Innovation Program (PAMIP). Acknowledgments to Prof. A.D. Rollett for supporting in securing funding for this research through PITA and PAMIP. Also, Kennametal Inc. is acknowledged for providing powder for this research. Partial support from the National Science Foundation under grant number DMR-2050916 is appreciated by MD and AM.

## **Author information**

### **Authors and Affiliations**

Department of Mechanical, Materials and Aerospace Engineering, Illinois Institute of Technology, 10 W 32<sup>nd</sup> Street, Chicago, IL, 60616, USA

Maciej Dorula, Meisam Khademitab, Mohammad Jamalkhani, Amir Mostafaei

## Contributions

Maciej Dorula: formal analysis, investigation, visualization. Meisam Khademitab: investigation, analysis. Mohammad Jamalkhani: investigation, analysis. Amir Mostafaei: conceptualization, methodology, investigation, visualization, supervision, project administration, funding acquisition, writing—original draft, review and editing.

## Corresponding author

Correspondence to Amir Mostafaei

## Conflicts of interest

The authors declare no competing interests.

## Availability of data and material

Data might be available upon request.

## References

- [1] A. Mostafaei, A.M. Elliott, J.E. Barnes, C.L. Cramer, P. Nandwana, M. Chmielus, Binder jet 3D printing - process parameters, materials, properties, modeling, and challenges, *Prog. Mater. Sci.* 119 (2021) 100707.
- [2] A. Mostafaei, P.R. De Vecchis, M.J. Buckenmeyer, S.R. Wasule, B.N. Brown, M. Chmielus, Microstructural evolution and resulting properties of differently sintered and heat-treated binder jet 3D printed Stellite 6, *Mater. Sci. Eng. C*. 102 (2019) 276–288.
- [3] A. Mostafaei, P. Rodriguez De Vecchis, E.L. Stevens, M. Chmielus, Sintering regimes and resulting microstructure and properties of binder jet 3D printed Ni-Mn-Ga magnetic shape memory alloys, *Acta Mater.* 154 (2018).
- [4] P. Nandwana, R. Kannan, D. Siddel, Microstructure evolution during binder jet additive manufacturing of H13 tool steel, *Addit. Manuf.* 36 (2020) 101534.
- [5] R. Kannan, P. Nandwana, Predicting sintering window during supersolidus liquid phase sintering of steels using feedstock analysis and CALPHAD, *Mater. Lett.* 304 (2021) 130648.
- [6] Z. Snow, R. Martukanitz, S. Joshi, On the development of powder spreadability metrics

and feedstock requirements for powder bed fusion additive manufacturing, *Addit. Manuf.* 28 (2019) 78–86.

- [7] N.D. Parab, J.E. Barnes, C. Zhao, R.W. Cunningham, A.D. Rollett, T. Sun, Real time observation of binder jetting printing process using high-speed X-ray imaging, *Sci. Rep.* (2019) 28–30.
- [8] R. Jiang, L. Monteil, K. Kimes, A. Mostafaei, M. Chmielus, Influence of powder type and binder saturation on binder jet 3D-printed and sintered Inconel 625 samples, *Int. J. Adv. Manuf. Technol.* 116 (2021) 3827–3838.
- [9] A. Mostafaei, P. Rodriguez De Vecchis, I. Nettleship, M. Chmielus, Effect of powder size distribution on densification and microstructural evolution of binder-jet 3D-printed alloy 625, *Mater. Des.* 162 (2019) 375–383.
- [10] S. Barui, H. Ding, Z. Wang, H. Zhao, S. Marathe, W. Mirihanage, B. Basu, B. Derby, Probing Ink-Powder Interactions during 3D Binder Jet Printing Using Time-Resolved X-ray Imaging, *ACS Appl. Mater. Interfaces.* 12 (2020) 34254–34264.
- [11] H. Miyanaji, N. Momenzadeh, L. Yang, Effect of printing speed on quality of printed parts in Binder Jetting Process, *Addit. Manuf.* 20 (2018) 1–10.
- [12] M. Ziae, N.B. Crane, Binder Jetting: A Review of Process, Materials, and Methods, *Addit. Manuf.* (2019).
- [13] K. Myers, A. Paterson, T. Iizuka, A. Klein, The Effect of Print Speed on Surface Roughness and Density Uniformity of Parts Produced Using Binder Jet 3D Printing, *Solid Free. Fabr. 2019 Proc. 30th Annu. Int.* (2019) 122–133.
- [14] D. Oropesa, R.W. Penny, D. Gilbert, A.J. Hart, Mechanized spreading of ceramic powder layers for additive manufacturing characterized by transmission x-ray imaging: Influence of powder feedstock and spreading parameters on powder layer density, *Powder Technol.* (2021) 117053.
- [15] I. Rishmawi, M. Salarian, M. Vlasea, Tailoring Green and Sintered Density of Pure Iron Parts using Binder Jetting Additive Manufacturing, *Addit. Manuf.* (2018).
- [16] E. Stevens, S. Schloder, E. Bono, D. Schmidt, M. Chmielus, Density variation in binder

jetting 3D-printed and sintered Ti-6Al-4V, *Addit. Manuf.* 22 (2018) 746–752.

- [17] D. Huber, L. Vogel, A. Fischer, The effects of sintering temperature and hold time on densification, mechanical properties and microstructural characteristics of binder jet 3D printed 17-4 PH stainless steel, *Addit. Manuf.* 46 (2021) 102114.
- [18] Z. Chen, W. Chen, L. Chen, D. Zhu, Q. Chen, Z. Fu, Influence of initial relative densities on the sintering behavior and mechanical behavior of 316 L stainless steel fabricated by binder jet 3D printing, *Mater. Today Commun.* 31 (2022) 103369.
- [19] M. Zago, N.F.M. Lecis, M. Vedani, I. Cristofolini, Dimensional and geometrical precision of parts produced by binder jetting process as affected by the anisotropic shrinkage on sintering, *Addit. Manuf.* 43 (2021) 102007.
- [20] B. Msalle, S. Neha, C. Shuaishuai, F.S. Halbeisen, F.M.T. Hans-Florian Zeilhofer, Evaluation of the Dimensional Accuracy of 3D-Printed Anatomical Mandibular Models Using, *J. Clin. Med.* 9 (2020) 1–18.
- [21] A.M. Elliott, P. Nandwana, D. Siddel, B.G. Compto, B.G. Compton, A Method for Measuring Powder Bed Density in Binder Jet Additive Manufacturing Process and the Powder Feedstock Characteristics Influencing the Powder Bed Density, *Solid Free. Fabr.* 2016. Proceeding (2016) 1031–1037.
- [22] U. Ali, Y. Mahmoodkhani, S. Imani Shahabad, R. Esmaeilizadeh, F. Liravi, E. Sheydaei, K.Y. Huang, E. Marzbanrad, M. Vlasea, E. Toyserkani, On the measurement of relative powder-bed compaction density in powder-bed additive manufacturing processes, *Mater. Des.* 155 (2018) 495–501.
- [23] L.I. Escano, N.D. Parab, L. Xiong, Q. Guo, C. Zhao, K. Fezzaa, W. Everhart, T. Sun, L. Chen, Revealing particle-scale powder spreading dynamics in powder-bed-based additive manufacturing process by high-speed x-ray imaging, *Sci. Rep.* 8 (2018) 15079.
- [24] C.G. Inkley, J. Lawrence, N.B. Crane, Impact of Controlled Prewetting on Part Formation in Binder Jet Additive Manufacturing, *Addit. Manuf.* (2023) 103619.
- [25] S. Wu, Y. Yang, Y. Huang, C. Han, J. Chen, Y. Li, D. Wang, Study on powder particle behavior in powder spreading with discrete element method and its critical implications for binder jetting additive manufacturing processes, (2023).

